Proceedings of the Second International Conference on Press-in Engineering 2021, Kochi, Japan – Matsumoto et al (eds)

A preliminary numerical model for erosion at the flow-soil interface based on the sediment transport model

Y. Yuan, F. Liang & C. Wang*
Tongji University, Shanghai, China

ABSTRACT: In recent years, using numerical methods to calculate fluid-particle interaction has become a new trend in scour research. To simulate the flow field and soil particle movements during scour, the traditional Euler equation and the sediment transport model were combined under the condition of single-phase flow in this study. Based on the assumptions and theories of Engelund and Bagnold, the whole calculation process from the particle initiation to the final deposition is completed. Through the sediment transport model and particle movement analysis, the topographic parameters of the grid can be updated, and the iterative calculation of the water-soil interface is realized. Using the above numerical model, the erosion process can be calculated under various test conditions, and the results can be validated by the test data. Finally, the parameter sensitivity of the model has also been discussed.

Keywords: *Erosion*, *Numerical model*, *Sediment transport*, *Flow-soil interface*

1 INTRODUCTION

Local scour under the condition of current is a typical physical phenomenon in water conservancy projects, which is common in projects such as wading bridges and offshore wind turbines. More than half of the bridge water damage problems are related to scour in recent years, which has also caused more and more scholars to pay attention to the scour problem (Søren, 2013; Escobar, 2018; Wang, 2017; Melville, 2000). Many experimental studies on this problem have been carried out (Ma, 2018; Liang, 2020; Lagasse, 2007). The flow structure in the local scour hole has been investigated using laboratory experiments, and the water flow's attenuation law around the foundation with the development of scour was obtained by scholars such as Rajaratnam (1977), Melville (1977), Graf (2002), Karim (2000) and Loópez (2008). To further clarify the scour mechanism under different water flow conditions, Dongol (1994) explored the law of scour evolution under the conditions of live water through flume tests, and the results are consistent with the test results of Chiew (1984) and Baker (1986). While Yang et al. (2010) conducted laboratory experiments on the phenomenon of river bed coarsening under the condition of clear water.

Although laboratory tests can effectively simulate on-site scour conditions to a certain extent, which intuitively shows the scour results under different working conditions, there are still shortcomings, such as time-consumption and high requirements for on-site equipment. It is worth noting that when the particle size of the soil is small, the water flow is prone to turbidity after scour occurs, which brings difficulties to observing the scour results. Therefore, numerical simulation can be a good choice as the research method for multi-condition analysis. The research results can be divided into two aspects: (1) Combining the standard k-ε turbulence model and Navier-Stokes equation to realize the numerical simulation of the three-dimensional complex flow field. The instantaneous change of the riverbed elevation coordinate during the scour process can be obtained (Zhou, 2016; Wang, 2014; Zhang, 2020; Zhu, 2011). (2) Exploring the local sediment transport situation based on the sediment initial motion theory (Einstein, 1942; Engelund, 1976a; Laursen, 1998; Wu, 2002). The above two studies mainly focused on the complex flow fields and sediment transport and carried out scour analysis and prediction based on the instantaneous results. However, these studies did not establish the relationship between flow, particle migration, and scour development, which considers the dynamic evolution of the erosion process. Meanwhile, most of the existing theoretical calculations and numerical analysis methods only consider the erosion effect of the flow, while the particle accumulations after the initial movement are usually ignored.

DOI: 10.1201/9781003215226-39

This research aims to establish the connection between water flow, particle migration, and scour development under a three-dimensional flow field. A preliminary numerical model for erosion at the flow-soil interface based on the sediment transport model is proposed. The effects of water erosion and particle accumulations on the riverbed elevation are comprehensively considered. Finally, taking the simple scour resistance test as an example, the numerical model was validated by previous SSRT results.

2 THEORETICAL MODEL

2.1 *Flow field governing equation*

The governing equations for fluids can be divided into continuity equations and motion equations. Among them, the continuity equation establishes an equal relationship between the sum of the inflow mass of the control surface and the mass increase in the control body from the perspective of mass conservation. According to Gauss's theorem, it can be written as the following tensor form:

$$\frac{\partial \rho}{\partial t}+\frac{\partial(\rho u_i)}{\partial x_i}=0 \tag{1}$$

where ρ is the fluid density, u_i is the flow velocity, t is the time.

The conservation of momentum is then used to calculate the fluid motion equation. For the convenience of calculation, it is usually assumed that the fluid is incompressible Newtonian fluid flow, and its motion equation is called Navier-Stokes equations (abbreviated as N-S equation). The ideal fluid N-S equation is used in this study, namely Euler's equation:

$$\begin{cases} f_x-\frac{1}{\rho}\frac{\partial \rho}{\partial x}=\frac{\partial u}{\partial t}+u\frac{\partial u}{\partial x}+v\frac{\partial u}{\partial y}+w\frac{\partial u}{\partial z} \\ f_y-\frac{1}{\rho}\frac{\partial \rho}{\partial y}=\frac{\partial v}{\partial t}+u\frac{\partial v}{\partial x}+v\frac{\partial v}{\partial y}+w\frac{\partial v}{\partial z} \\ f_z-\frac{1}{\rho}\frac{\partial \rho}{\partial z}=\frac{\partial w}{\partial t}+u\frac{\partial w}{\partial x}+v\frac{\partial w}{\partial y}+w\frac{\partial w}{\partial z} \end{cases} \tag{2}$$

where u, v, w are the flow velocity components in the x, y, z-axis directions, respectively.

2.2 *Plane sediment transport equation*

The first step in the sediment calculation model is to judge the initiation of the surface particles under the calculated flow field conditions. So it is necessary to conduct a force analysis. Affected by water flow, surface particles are mainly subjected by drag force F_D, upward force F_L, and gravity W (Einstein, 1942; Laursen, 1998). The initial movement occurs under the combined action of the three forces, and the calculation expressions are as follows:

$$F_D=C_D\cdot\frac{\pi D^2}{4}\cdot\frac{\rho u_0^2}{2} \tag{3}$$

$$F_L=C_L\cdot\frac{\pi D^2}{4}\cdot\frac{\rho u_0^2}{2} \tag{4}$$

$$W=\frac{\pi D^3}{6}\cdot(\gamma_s-\gamma) \tag{5}$$

where C_D is the drag coefficient, C_L is the uplift coefficient, u_0 is the flow velocity acting on the surface of the river bed, D is the particle size, γ_s is the dry unit weight, and γ is the unit weight of soil.

When the instantaneous drag force, F_D, is greater than the particle interaction force, the surface particles will occur initial movement, which can be judged according to the following equation:

$$F_D=f\cdot(W-F_L)=(W-F_L)\cdot\tan\varphi \tag{6}$$

where φ is the underwater repose angle of the surface particles.

After the initiation, the surface particles are continuously eroded by flow and transported downstream. At this moment, the scour begins to occur. To realize the quantitative calculation of the scour development process, the formula of sediment transport rate proposed by Engelund (1976b) is used to calculate the particle loss. Then the relationship between the elevation of the riverbed and the particle migration can be established. When calculating sediment transport, Engelund simplified the sediment particles into spheres. There are $1/D^2$ sediments in the unit area at this time, and it is assumed that p% of them will undergo initial movement. So, the moving sediment number for per unit area n is:

$$n=\frac{p}{D^2} \tag{7}$$

Eq. (8) shows the formula proposed by Engelund, which can calculate the sediment transport rate. Combining calculation assumptions, n and u_b are the critical parameters in theoretical and numerical calculations. Meanwhile, n is used to calculate the deformation of mesh nodes, and u_b is for particle migration. The drag force, F_D, and friction resistance of the particles, $\overline{\mathrm{F_x}}$, after the initial movement, can be calculated according to Eq. (9) and Eq. (10).

$$g_b=\frac{\pi D^3}{6}\gamma_s\cdot\frac{p}{D^2}\overline{u_b} \tag{8}$$

$$F_D=C_D\cdot\frac{\pi D^2}{4}\cdot\frac{\rho}{2}\cdot(\alpha_0 U_*-\overline{u_b})^2 \tag{9}$$

$$\overline{F_x} = \frac{\pi D^3}{6}(\gamma_s - \gamma) \cdot \beta \tag{10}$$

where g_b is the unit sediment transport rate and $\overline{u_b}$ is the initial velocity of particle movement, β is the friction coefficient, and $\alpha_0 U_*$ reflects the flow velocity at which the bed load moves near the bed surface. If the distance from the bed surface when the bed load moves are about twice the particle size, the recommended value range for α_0 is [6,10].

When the scour reaches the equilibrium state, the drag force is equal to the friction force, Eq. (9) and Eq. (10) can be combined:

$$\frac{\overline{u_b}}{U_*} = \alpha_0 \cdot \left(1 - \sqrt{\frac{\Theta_0}{\Theta}}\right) \tag{11}$$

where, Θ_0 is equivalent to the water flow intensity value corresponding to the condition that the surface particles just no longer move ($\overline{u_b} = 0$), which can be connected with Θ_c; Θ is the flow intensity parameter, which can be calculated as follows (Albertson, 1958):

$$\Theta = \frac{\tau_0}{(\gamma_s - \gamma)D} = \frac{U_*^2 \rho}{(\gamma_s - \gamma)D} \tag{12}$$

where τ_0 is the shear stress of flow.

In particular, the intensity of the water flow when the surface particles just reach the initial motion conditions is recorded as Θ_c. Then Eq. (12) can be further derived that:

$$\Theta_0 = \frac{4\beta}{3\alpha^2 C_D} \tag{13}$$

After establishing a connection based on the measured data, Eq. (11) can be written as the following equation:

$$\frac{\overline{u_b}}{U_*} = \alpha_0 \cdot \left(1 - 0.7\sqrt{\frac{\Theta_c}{\Theta}}\right) \tag{14}$$

On this basis, combined with the concept of Bagnold (from the perspective of energy) (Bagnold, 1966), the shear stress τ_0 of the sand-laden flow is composed of two parts, the particle shear force T and the flow shear force τ' of the static riverbed, and it is considered that the flow shear force τ' is equal to the initial shear force τ_c of the sediment particles. The particle shear force is generated by particle friction, which can be obtained from Eq. (15):

$$T = n\overline{F_x} \tag{15}$$

From this, the moving sediment number for per unit area n and the local grid elevation change ΔH can be derived:

$$n = \frac{6}{D^2 \pi \beta} \cdot (\Theta - \Theta_c) \tag{16}$$

$$\Delta H = \frac{6D}{\pi \beta} \cdot (\Theta - \Theta_c) \tag{17}$$

2.3 *Inclined plane sediment transport equation*

However, the actual riverbed conditions are not ideally flat. Furthermore, with the occurrence of scour, the riverbed topography will continue to change. The scour calculation method derived in the planar state often cannot meet complex topographic changes. So it is necessary to derive the calculation formula on the slopes. It is worth noting that, unlike the movement in a flat state, particle movement under slope conditions is more complicated (as shown in Figure1). It is no longer a simple linear motion but should be considered in several stages for analysis.

In the derivation of the plane condition, the component force of the particle gravity along the water flow direction is ignored. When the river bed condition is a slope, the existence of the gravity component will promote the initial movement of the particles, which will affect the subsequent development of scour. In order to clarify the particle movement under slope conditions, this study established

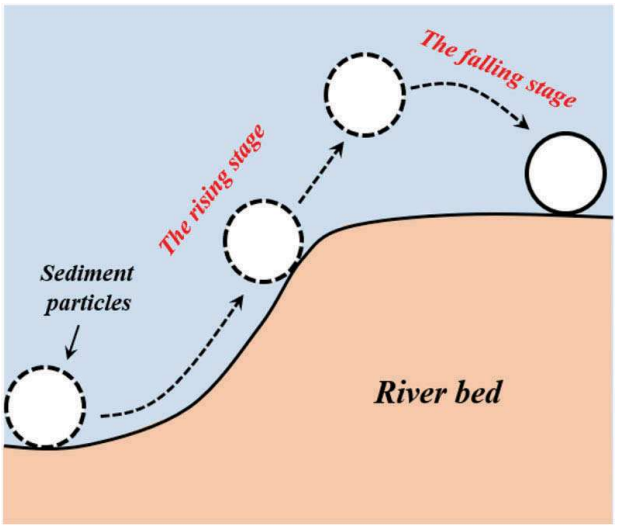

Figure 1. Schematic diagram of particle movement on a slope.

a standard particle slope force model. The force analysis diagram is shown in Figure 2. It is assumed that the slope angle is θ, the particles will initially move along the direction at an angle of α to the horizontal axis of the slope under the action of the water flow.

Affected by the slope angle and the current direction, the drag force and the gravity will form a component force, F, with a certain angle with the horizontal axis. The equation for determining the initial movement of particles at this time is as follows:

$$F_D = (W\cos\theta - F_L)\cdot\tan\varphi \tag{18}$$

Similarly, the calculation formula of the moving sediment number for per unit area n and the local grid elevation change ΔH also needs to be modified:

$$n = \frac{6}{D^2\pi\beta\cos\theta}\cdot(\Theta-\Theta_c) \tag{19}$$

$$\Delta H = \frac{6D}{\pi\beta\cos\theta}\cdot(\Theta-\Theta_c) \tag{20}$$

Eq. (19) and Eq. (20) can calculate the erosion depth after the surface particle eroded by the flow. However, the sedimentation will also affect the final elevation of each grid node when the scour reaches the equilibrium status. To determine the impact of particle sedimentation on the scour development, it is necessary to analyze the subsequent movement of particles after leaving the soil surface. It can be seen in Figure 1 that when the riverbed is in a slope state, the particles can be roughly divided into two stages after the initiation. In the first stage, called the ascending stage, the particles continue to move with the flow after leaving the soil surface but slowly deposit due to gravity. In the second stage, which is called the falling stage, the particles fall to the soil surface, and the particles show a state of near-surface motion. Limited by force between the particles, the particles quickly reach a stable equilibrium state. For the convenience of analysis, the water flow velocity and particle movement velocity are decomposed into U_{*x}, U_{*y}, $u_{x,}$ and u_y along the x-axis and y-axis. When the particle starts on the inclined plane, the component of particle motion velocity along the z-axis is recorded as u_z. When the particle movement is in the first stage, it can be known from the momentum equation:

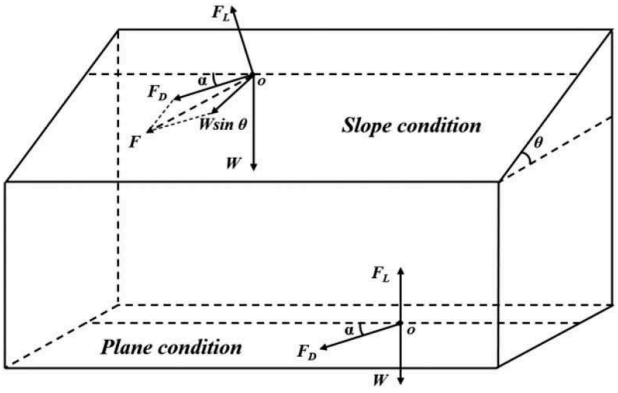

Figure 2. The force analysis diagram.

$$\begin{cases} F_x = m\frac{\partial u_x}{\partial t} \\ F_y = m\frac{\partial u_y}{\partial t} \\ -F_z - W = m\frac{\partial u_z}{\partial t} \end{cases} \tag{21}$$

where,

$$\begin{cases} F_x = C_D\cdot\frac{\pi D^2}{4}\cdot\frac{\rho}{2}\cdot(U_{*x}-u_x)\left|U_{*x}-u_x\right| \\ F_y = C_D\cdot\frac{\pi D^2}{4}\cdot\frac{\rho}{2}\cdot\left(U_{*y}-u_y\right)\left|U_{*y}-u_y\right| \\ F_z = C_D\cdot\frac{\pi D^2}{4}\cdot\frac{\rho}{2}\cdot u_z^2 \end{cases} \tag{22}$$

Specially, the transformation of partial differential equations can be considered:

$$\frac{du_z}{dt} = \frac{1}{t}\frac{dz}{dt} - \frac{u_z}{t} \tag{23}$$

Eq. (23) can be used to transform Eq. (21) into a differential equation related to displacement and time. Through iterative calculation, the movement state of the particles along with the x and y directions when the particles sink to the surface of the soil can be calculated. The movement of the particles enters the second stage, and the momentum equation at this time is established:

$$\begin{cases} F_x - \overline{F_x} = m\frac{\partial u_x}{\partial t} \\ F_y - \overline{F_y} = m\frac{\partial u_y}{\partial t} \end{cases} \tag{24}$$

where, $\overline{F_x}$and $\overline{F_y}$ are the component of resistance along the x- and y-axis, which can be calculated as follows:

$$\begin{cases} \overline{F_x} = \frac{\pi D^3}{6}(\gamma_s-\gamma)\cdot\beta\cdot\cos\theta\cdot\sin\alpha \\ \overline{F_y} = \frac{\pi D^3}{6}(\gamma_s-\gamma)\cdot\beta\cdot\cos\theta\cdot\cos\alpha \end{cases} \tag{25}$$

Combining Eqs. (25) and (23), iteratively solve the displacements in the x and y directions to determine the coordinates of particle accumulation. Then using Eq. (20) to calculate the elevation change, which realizes the dynamic update of the grid node elevation.

3 CASE ANALYSIS AND MODEL ESTABLISHMENT

3.1 *Simple Scour Resistance Test (SSRT)*

As a new type of test method for studying meso-scour (Wang, 2018), the simple scour resistance test has dramatically alleviated the drawbacks of the flume experiment due to its convenience and time-saving process. Through the rotation of the blade, different local flow field conditions can be simulated. With the test results for various soil conditions, the performance of different soil properties is obtained. To validate the accuracy and applicability of the theoretical model and numerical calculations, we selected SSRT experiments as a example because it involves the results and processes of both erosion and deposit. The test device comprises the following three parts: power device, transmission device, and sample container. The schematic diagram of the structure is shown in Figure 3. The device effectively simulates the actual flow field conditions during scour, and restores soil erosion and particle migration. The inner diameter of the sample container is 90mm, the total height is 128mm, and the thickness of the soil sample in the container is 40mm. The blades used are 76mm wide and 22mm high. The speed range is 0-150r/min, and the corresponding simulated flow velocity range is 0-0.6m/s.

3.2 *Model establishment and calculation process*

Unlike the flume tests, this method also has apparent mesoscopic particle erosion and accumulation phenomena. In order to simulate the SSRT experiment well through the model, the deposition of particles needs to be considered. which is rarely considered in traditional methods. However, the scour theory proposed in the previous section satisfies the numerical calculation requirements of SSRT well.

The numerical calculation simulated four soil samples with a median diameter of 0.075mm, 0.25mm, 0.5mm, and 2mm under the conditions of the rotation speed of 70r/min and 90r/min. To simplify the description, take the speed condition of 70r/min as an example to introduce the overall modeling calculation process. This study mainly focuses on calculating local scour using the sediment transport formula, which does not have such high accuracy requirements for complex flow fields. Therefore, in order to improve the calculation efficiency, combined with the theoretical basis of the previous section, numerical calculations are carried out using coupled modeling of COMSOL and MATLAB. The schematic diagram and meshing of the COMSOL model are shown in Figure 4. The k-ε model in COMSOL is used to calculate and update the real-time flow

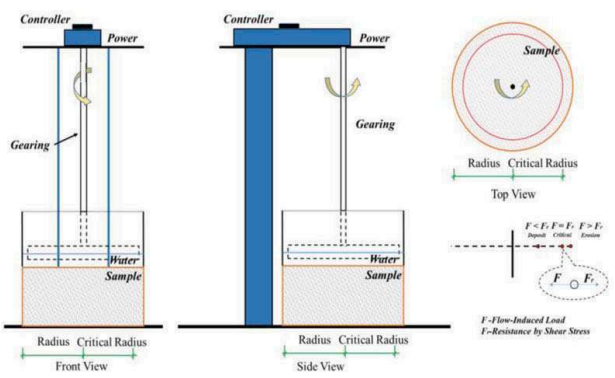

Figure 3. SSRT setup (Wang 2018).

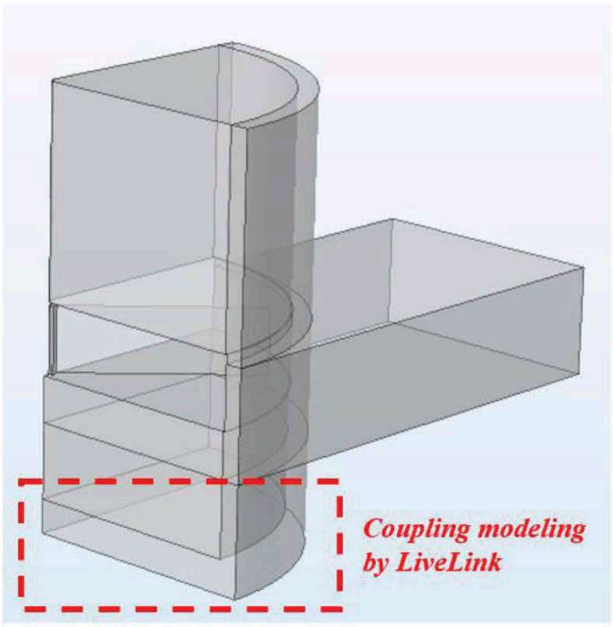

(a) Model building

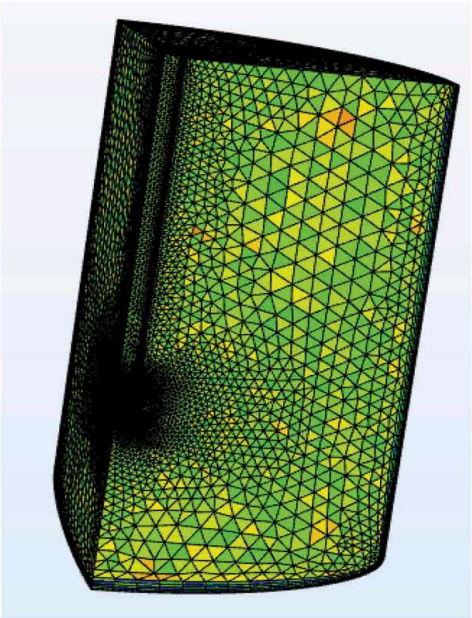

(b) Meshing result

Figure 4. Model building and meshing result.

field. In each iterative calculation, for the flow field calculation results of COMSOL, the movement calculation of sediment particles is realized through MATLAB. After obtaining the instantaneous riverbed elevation changes, the model parameters can be adjusted through the LiveLink module. As shown in Figure 4(a), the red dashed area is the coupling modeling area. The numerical model is established as a 1/4 prototype model, which maximally reduces the calculation time.

A grid is the basis of numerical simulation calculation. Grid division determines the division of the calculation domain and the degree of dispersion of the control equations, and its scale determines the stability and accuracy of the calculation. Therefore, the division of the grid is essential in numerical simulation. In particular, the flow field around the blades in this simulation is very complicated, which puts higher requirements on the grid division. As shown in Figure 4(b), in order to ensure the accuracy of the calculation results, the meshes of the model boundary and the surrounding area of the blade are locally refined.

Figure 5 shows the numerical calculation results of the local flow field calculated in one iteration. The cross-sectional flow field distribution is shown in Figure 5(a), while Figure 5(b) shows the flow field distribution of the sidewall. It can be seen that there is an apparent secondary flow phenomenon in the cross-sectional flow field under the action of the blade rotating. The sidewall flow field presents a band-like diffusion distribution from the center to the upper and lower sides. Such calculation results are highly consistent with the previous research results of many scholars (Zhang, 2020; Einstein, 1926), verifying the reliability of the flow field calculation results to a certain extent.

The flow field conditions calculated by COMSOL are used as the initial flow field conditions, and the scour theory mentioned above is used to realize the iterative calculation of the scour process. Figure 6 shows the shape of the scour result drawn based on the scour calculation results after one iteration. Affected by the secondary flow, particles eroded by the flow continue to gather into the central area of the intermediate device. Apparent zoning phenomena (eroded area and deposition area) appeared in the scour pattern, consistent with the experimental observation results (Wang, 2018). As the scour iteration progresses, erosion and accumulation phenomena continue to develop and appear as an apparent hat shape at last.

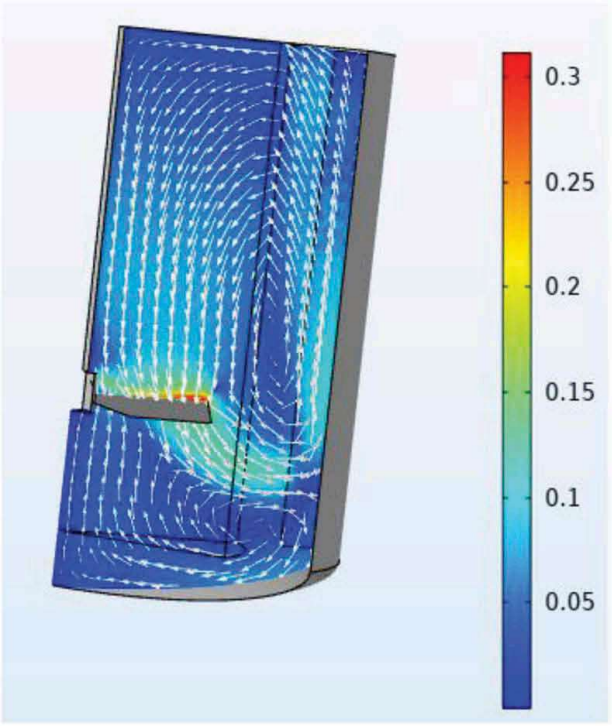

(a) Cross-section

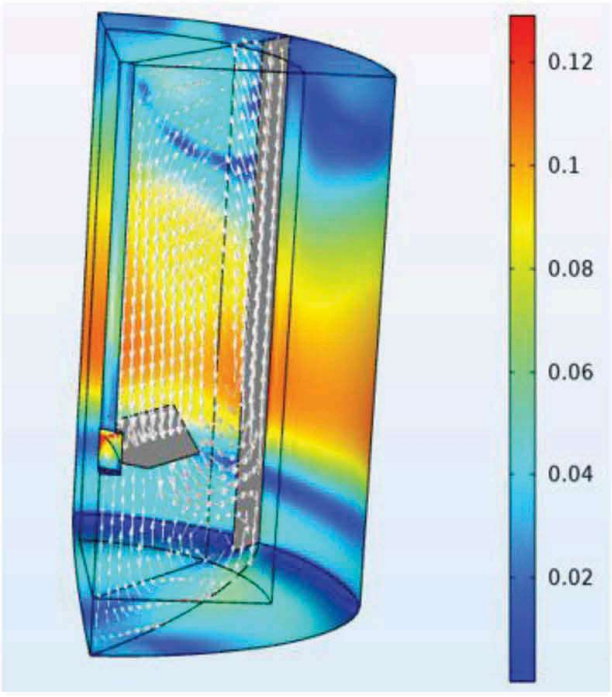

(b) Sidewall

Figure 5. Flow field calculation results.

4 RESULTS AND ANALYSIS

4.1 *Influence of particle size*

Figure 7 shows the scour development curve of the numerical simulation and the SSRT test of soil with different particle sizes under rotation speed of 70rpm, where Figure 7(a) compares the result of erosion depth, and Figure 7(b) for the deposition height. Since the flow field conditions in the numerical calculation are all instantaneous loading, which assumes that the water flow velocity reaches the test

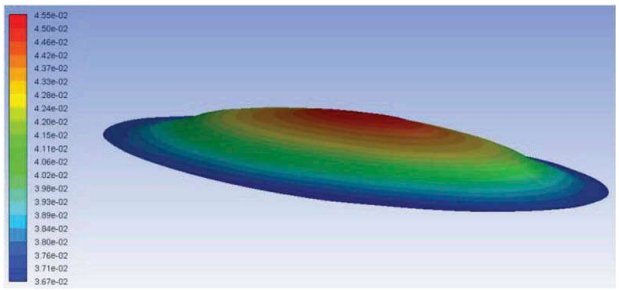

Figure 6. Scour simulation results after one iteration.

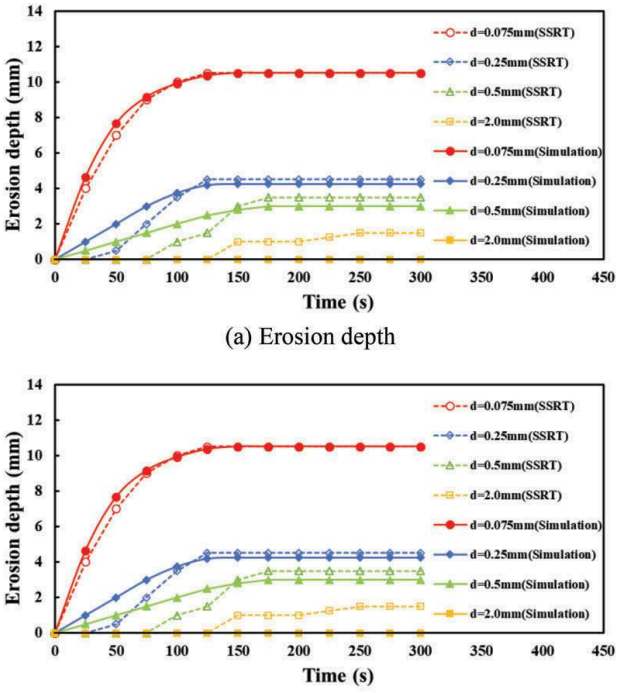

(a) Erosion depth

(b) Deposition height

Figure 7. Scour development curve of numerical simulation and SSRT at 70rpm.

requirement of 70rpm at the beginning of the test, the numerical simulation curve develops rapidly from 0s. However, there are specific differences in actual test conditions. After the blade rotates, the flow field conditions will slowly generate the expected conditions. As the flow velocity increases, only some of the particles have initiated. Therefore, the initial slope of the test curve is delayed than the numerical results. This phenomenon is more apparent in the case of large particles than small ones. With the continuous development of the scour depth, the intensity of the water flow decays along the depth direction. When the strength caused by the flow is equal to the erosion resistance of the soil particles, the scour reaches an equilibrium status. Therefore, the differences at the beginning will not affect the final scour depth and deposition height. The numerical model can provide reliable equilibrium erosion depth and deposition height.

Comparing the erosion depth and accumulation height after the erosion reaches the equilibrium status, the numerical calculation result of the soil sample with a particle size of 0.075 mm is approximately equal to the test results. When the median particle size is changed to 0.25mm and 0.5mm, the accuracy of the numerical simulation will decrease. In general, the numerical calculation method used in this study has higher accuracy for small-particle soil samples than large ones. This is because the grid node elevation in the calculation model uses the particle size as the minimum standard calculation unit. Calculated results (erosion depth or deposit height) less than the calculation unit would be automatically ignored in every step. Hence, the deviation of simulation results for large particles is larger than small ones. Especially, when the particle size is 2.0mm, it can be known from Eq. (18) that the particles will not initiate at this time, which makes the calculated erosion depth and deposition height 0. After disturbed by the water flow, the particles may roll over under the flow condition. Therefore, there will be a certain erosion depth and deposition height in the experiment but are observed smaller than the size of a single particle.

4.2 *Influence of rotating velocity*

The comparisons of numerical simulation and test results at the speed of 70rpm and 90rpm are shown in Table 1 and Table 2. After the water flow rate increased, the numerical calculation results for different particle sizes have changed to various degrees. At the speed of 70rpm, for soil samples with particle sizes of 0.25mm and 0.5mm, the calculation deviations of the erosion depth are 5.6% and 14.3%. When the speed is 90rpm, the deviation of the erosion depth under two soil conditions becomes 5.6%

Table 1. Comparison of numerical simulation and test results at 70r/min.

		Erosion depth (mm)			Deposition Height (mm)		
Cases	D_{50} (mm)	SSRT	Simulation	Deviation	SSRT	Simulation	Deviation
1	0.075	10.5	10.5	0%	12.0	12.0	0%
2	0.25	4.5	4.25	5.6%	10.5	10.25	2.4%
3	0.5	3.5	3.0	14.3%	7.5	7.0	6.7%

Table 2. Comparison of numerical simulation and test results at 90r/min.

		Erosion depth (mm)			Deposition Height (mm)		
Cases	D_{50} (mm)	SSRT	Simulation	Deviation	SSRT	Simulation	Deviation
4	0.25	9.0	9.5	5.6%	13.0	13.5	3.8%
5	0.5	5.0	5.5	10.0%	10.0	11.0	10.0%

and 10.0%, and the calculation accuracy is higher than that under the low-velocity condition. However, the simulation results of the deposition depth show an opposite situation. It increased from 2.4% and 6.7% at 70rpm to 3.8% and 10% at 90rpm. Nevertheless, the maximum numerical simulation deviations of both the erosion depth and the deposition height of the two soil samples did not exceed 10%. This verifies the reliability and applicability of the numerical calculation method for different flow rate conditions to a certain extent.

5 CONCLUSIONS

Based on the sediment transport model, a method for calculating the erosion depth of particles under is derived. From the perspective of conservation of momentum, the migration and accumulation process of particles after initiation is discussed. Based on these, a preliminary numerical model for erosion at the flow-soil interface was proposed. The calculation model is then used for the numerical simulation of the SSRT test, which explores the difference between the numerical simulation results and the test results, and draws the following conclusions:

1. The scour numerical model proposed in this study establishes the relationship between water flow, particle migration, and scour development under the conditions of a three-dimensional flow field. It performs well under most scour conditions.
2. The load loading mode of the flow field assumed by the model is different from the practice. The initial erosion development simulation curve is different from the experimental one, but it does not affect the simulation accuracy of the final erosion depth and deposition depth.
3. The numerical simulation accuracy is related to the flow field conditions and particle sizes in the experiments. For the same flow field conditions, the smaller the particle sizes, the higher the model's accuracy. With the increase of the flow rate, the method performs well for the small particle size soil show strong stability. For large particles, the results of numerical calculations are generally reliable, except for those that will not initiate.
4. The model can study the accumulation process of particles, which can simulate the process with evident particle accumulation, e.g., what happens in the SSRT test.

ACKNOWLEDGEMENTS

This work was supported by the National Natural Science Foundation of China (Grant No. 51908421) and "Chen Guang" project supported by Shanghai Education Development Foundation and Shanghai Municipal Education Commission (Grant No. 19CG21). Financial support from these organizations is gratefully acknowledged.

REFERENCES

Albertson, M.L., Simons, D.B., Richardson, E.V. 1958. Discussion of "mechanics of sediment-ripple formation" by H. L. Liu. *Journal of Inorganic & Nuclear Chemistry*, 39(8), 1437–1442.

Bagnold, R.A. 1966. An Approach to the Sediment *Transport Problem From General Physics*. U.S. Geol. Survey, Prof. Paper No.422, 1996, p.37.

Baker, R.E. 1986. Local scour at bridge piers in non-uniform sediment. Rep.No402, School of Eng., University of Auckland, Auckland, New Zealand, 1986.

Chiew, Y.M. 1984. Local scour at bridge piers. Rep.No.355, University of Auckland, Auckland, New Zealand, 1984.

Dongol, D.M.S. 1994. Local scour at bridge abutments. Rep. No.544, School of Eng., University of Auckland, Auckland, New Zealand.

Einstein, A. 1926. Die ursache der manderbildung der flulufe und des sogenannten baerschen gesetzes. *Naturwissenschaften*, 14(11), 223–224.

Einstein, H.A. 1942. Formulas for the transportation of bed load. *Transactions of the American Society of Civil Engineers*, 107, 561–597.

Engelund, F., Fredsee, J. 1976a. A sediment transport model for straight alluvial channels. Iowa Publishing. Sediments. IFCEE 2018.

Engelund, F., Jørgen, F. 1976b. A sediment transport model for straight alluvial channels. *Hydrology Research*. 7(5), 293–306.

Escobar, A., Negro, V., López-Gutiérrez, J.S. 2018, et al. Assessment of the influence of the acceleration field on scour phenomenon in offshore wind farms. *Renewable Energy*. 136, 1036–1043.

Graf, W.H., Istiarto, I. 2002. Flow pattern in the scour hole around a cylinder. *Journal of Hydraulic Research*, 40 (1):13–20.

Karim, O.A., Ali, K.H.M. 2000. Prediction of flow patterns in local scour holes caused by turbulent water jets. *Journal of Hydraulic Research*, 38(4):279–287.

Lagasse, P.F., Clopper, P.E., Zevenbergen, L.W., Girard, L. W. 2007. National cooperative highway research program (NCHRP REPORT 593): Countermeasures to protect bridge piers from scour. Washington D.C.: Transportation Research Board.

Laursen, E.M., Papanicolaou, A.N., Cheng, N.S., et al. 1998. Pickup Probability for sediment entrainment. *Journal of Hydraulic Engineering*, 125(7):789–789.

Liang, F.Y., Zheng, H.B., Zhang, H. 2020. On the pile tension capacity of scoured tripod foundation supporting offshore wind turbines. Applied Ocean Research, 35:295: 306.

Loópez, R., Barragaón. 2008. Equivalent roughness of gravel-bed rivers. *Journal of Hydraulic Engineering*, 134(6):847–851.

Ma, H.W., Yang, J., Chen, L.Z. 2018. Effect of scour on the structural response of an offshore wind turbine supported on tripod foundation. *Applied Ocean Research*, 73: 179–189.

Melville, B.W., Raudkivi, A.J. 1977. Flow characteristics in local scour at bridge piers. J*ournal of Hydraulic Research*, 15(4):373–380.

Melville, B.W., Coleman, S.E. 2000. Bridge scour. *Water Resources Publications*, Colorado, USA.

Rajaratnam, N., Berry, B. 1977. Erosion by circular turbulent wall jets. *Journal of Hydraulic Research*, 15(3):277–289.

Søren, P.H.S., Ibsen, L.B. 2013. Assessment of foundation design for offshore monopiles unprotected against scour. *Ocean Engineering*, 63:17–25.

Wang, C., Yu, X., Liang, F.Y. 2017. A review of bridge scour: mechanism, estimation, monitoring and countermeasures. *Natural Hazards*, 87(3):1881–1906.

Wang, C., Yu, X., Liang, F.Y. 2018. A preliminary design of apparatus for scour resistance test in riverbed. International Foundations Congress and Equipment Expo (IFCEE), ASCE, Orlando, U.S.A., 746–757.

Wang, J.J., Ni, F.S. 2014. Numerical simulation of coarse-sandy bed scour by 2D vertical submerged jet. *Science Technology and Engineering*, 14 (3): 108–111. (In Chinese)

Wu, F.C., Lin, Y.C. 2002. Pickup probability of sediment under log-normal velocity Distribution. *Journal of Hydraulic Engineering*, 128(4):438–442.

Yang, F., Liu, X., Cao, S., et al. 2010. Bed load transport rates during scouring and armoring processes. *Journal of Mountain Science*, 7(3):215–225.

Zhang, W., Zapata, M.U., Bai, X., et al. 2020. Three-dimensional simulation of horseshoe vortex and local scour around a vertical cylinder using an unstructured finite-volume technique. *International Journal of Sediment Research*, 35 (2020):295–306.

Zhou, L.D. 2016. Scour mechanism and characteristics of vortex -induced vibrations of a submarine free spanning pipelines. Tianjin: Tianjin University. (In Chinese)

Zhu, Z.W., Liu, Z.Q. 2011. Three-dimensional numerical simulation of local scour around cylindrical bridge piers. *China Journal of Highway and Transport*, 24 (02):42–48. (In Chinese)